Charge transport gap in graphene antidot lattices

A. J. M. Giesbers,[1,*] E. C. Peters,[1] M. Burghard,[1] and K. Kern[1,2]
[1]*Max Planck Institute for Solid State Research, Heisenbergstrasse 1, D-70569 Stuttgart, Germany*
[2]*Institute de Physique de la Matière Condensée, Ecole Polytechnique de Lausanne, CH-1015 Lausanne, Switzerland*
(Received 13 April 2012; revised manuscript received 28 June 2012; published 26 July 2012)

Graphene antidot lattices (GALs) offer an attractive approach to band-gap engineering in graphene. Theoretical studies indicate that the size of the opened gap is sensitive to the shape, size, and architecture of the nanoholes introduced into the graphene sheet. We have investigated the temperature-dependent electrical conductivity of GALs comprising 50-nm-diameter nanoholes with a pitch of 80, 100, and 200 nm, respectively. The data reveal the presence of localized states within a transport gap, whose interactions lead to a soft Coulomb gap and associated Efros–Shklovskii variable range hopping (ES-VRH). This conduction type is preserved upon application of magnetic fields up to 1 Tesla, above which a transition to Mott variable range hopping occurs. Such a crossover can alternatively be introduced at zero magnetic fields by increasing either the nanohole spacing or the gate-controlled carrier concentration. Furthermore, at intermediate magnetic fields, the hopping exponent assumes a value of 2/3, as predicted by percolation theory for ES-VRH under this condition.

DOI: 10.1103/PhysRevB.86.045445 PACS number(s): 72.80.Vp, 72.20.Ee

I. INTRODUCTION

The strong potential of graphene for future electronic applications and its fundamental physics have attracted extraordinary attention.[1,2] However, despite considerable recent progress in the synthesis and controlled manipulation of graphene, its lack of a band gap has posed strong limitations on the development of technologically relevant graphene-based electronic devices.[1,2] One possibility to overcome this hurdle is the use of graphene nanoribbons (GNRs),[3,4] or graphene antidot lattices (GALs).[5–9] The latter represent an interconnected array of GNRs within a graphene sheet and correspondingly allow for enhanced driving currents. Like their counterparts defined within semiconductor heterostructures, GALs are expected to exhibit a wide range of intricate transport properties, especially in magnetic fields where the competing length scales lead to rich physics. According to numerous theoretical studies,[5–9] GALs offer the principal possibility of tuning the size of the gap via the antidot lattice parameters, specifically the diameter, shape, and separation of the nanoholes. In particular, it has been predicted that the size of the band gap in GALs scales inversely with the neck width.[9] While experimental studies have provided hints for band gap opening in GALs with neck widths of the order of 20 nm,[10] only little is known about the influence of the geometry of the nanohole array on the charge transport behavior of GALs. Furthermore, the nature of the band gap, i.e. whether it is robust or rather represents a charge transport gap arising from localization due to disorder, has not yet been established. In this paper, we explore in detail the band gap characteristics of GALs with different geometries using temperature-, concentration-, and magnetic field-dependent electrical transport studies. As summarized in Table I, the diameter of the circular nanoholes in the investigated samples was kept at 50 nm, while the holes were arranged in either hexagonal or cubic geometry, and their (center-to-center) separation was varied between 80 and 200 nm.

II. EXPERIMENTAL RESULTS AND DISCUSSION

A. Sample preparation

The graphene sheets were deposited by hot exfoliation onto silicon substrates covered with a 300-nm layer of thermally grown SiO_2. This method is similar to standard exfoliation[11] except that the deposition on the Si/SiO_2 substrate is done at an elevated temperature to gain a higher yield of monolayers. The substrates were first heated to 160 °C and then left to cool down to about 60 °C, at which temperature the graphene was deposited from the scotch tape. Afterwards, the samples were annealed in argon at 250 °C, which was directly followed by a first e-beam lithography (EBL) step to define four-probe Cr/Au (2/100 nm) contacts. In a second EBL step, the etching mask for the nanohole pattern was defined within a single layer of poly(methyl methacrylate) (PMMA). Subsequently, the graphene underneath the exposed areas was etched away by reactive ion etching. All electrical measurements on the graphene antidot lattices were preformed with standard ac techniques at low enough currents to avoid heating effects in the high-resistance regime. In total, three different substrates with, in total, seven GAL devices were investigated. The field-effect mobility of the GAL devices was found to reach values up to 5000 cm^2/Vs at 4 K. The charge neutrality points of both the antidot lattice and pristine graphene samples occurred around a back-gate voltage of 10 V, indicating the good quality of the GALs even without annealing.

B. Transport in graphene antidot lattices at $B = 0$ T

Figure 1(a) shows the temperature-dependent conductivity at the charge neutrality point (CNP) of a GAL with 100-nm separation between cubically arranged nanoholes (sample no. 4). From the dependence of the conductance on the carrier concentration, it is apparent that, at low temperatures, a (transport) gap opens at the Dirac point [see Fig. 1(b)].[6,8–10] With rising temperature [Fig. 1(a)], the conductivity at the

 ©2012 American Physical Society

TABLE I. Device parameters and extracted physical values for seven different graphene antidot lattice devices and a pristine graphene sample under zero magnetic field for comparison.

Number	Diameter/spacing lattice type (nm)	CNP (V)	ν	T_0 (K)	$\varepsilon\xi$ (nm)	ξ (nm)	R_{hop} (nm) at 10 K	E_{hop} (K; meV)	E_{CG} (K; meV)
1	50/80 cub	11.5	0.47 ± 0.04	360	130	54	81	30.0; 2.6	36.4; 3.14
2a	50/100 cub annealed	5.5	0.47 ± 0.04	140	334	139	130	18.7; 1.6	14.1; 1.22
2b	50/100 cub	12.5	0.50 ± 0.03	98	480	200	156	15.7; 1.4	9.9; 0.85
3	50/100 hex	12.0	0.46 ± 0.05	70	667	278	184	13.2; 1.1	7.1; 0.61
4	50/100 cub	10.6	0.49 ± 0.03	63	742	309	194	12.6; 1.1	6.4; 0.55
5	50/100 cub	18.0	0.55 ± 0.05	35	1337	557	260	9.4; 0.8	3.5; 0.30
6	50/100 cub	13.8	0.51 ± 0.03	33	1418	591	268	9.1; 0.8	3.3; 0.28
7	50/200 cub	10.0	0.26 ± 0.03	0.5	$g_0\xi^2 = 17$ K^{-1}			1.2; 0.1	
8	No dots	8.0							

CNP increases exponentially according to

$$\sigma = \sigma_0 \, e^{-(T_0/T)^{\nu}}, \quad (1)$$

where $\sigma_0 \approx e^2/h$.[12] Here T_0 and the exponent ν depend on the conduction mechanism. Fitting this equation to the measured temperature-dependent conductivity [see Fig. 1(a)] yields an exponent of $\nu = 0.49 \pm 0.03$ and $T_0 = 63$ K. To exclude possible bias voltage dependencies in the ac-transport data, we performed complementary dc electrical measurements, which revealed a negligible influence of the bias on the temperature-dependent conductivity and gave similar results for the exponent, specifically $\nu = 0.48 \pm 0.03$ and $T_0 = 58 \pm 10$ K. The corresponding values for the other samples are listed in Table I. For all samples, except no. 7 with the largest nanohole separation (200 nm), the exponent is close to 1/2, which is indicative of two-dimensional Efros–Shklovskii variable range hopping (ES-VRH) between localized states. These localized states are most likely positioned at the nanohole edges.[6,12] For ES-VRH transport, T_0 is given by

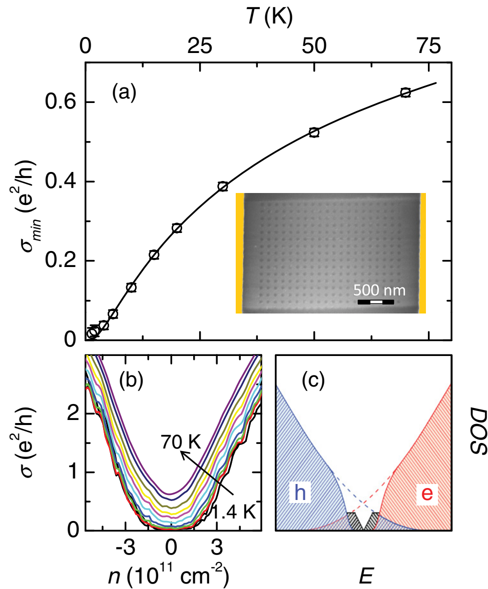

FIG. 1. (Color online) Analysis of the temperature dependence of conductivity and gate dependence of the Coulomb gap. (a) Conductivity of sample no. 4, comprising 50-nm-sized nanoholes with 100-nm spacing, at the charge neutrality point ($V_G = 10.6$ V) as a function of temperature. The solid line is a fit of the experimental data using the general thermal activation dependency valid for hopping conduction (exponent $\nu = 0.49 \pm 0.03$). The inset shows a scanning electron micrograph of the patterned graphene between two gold contacts serving as voltage probes. (b) The conductance through sample no. 4 as a function of back-gate voltage for various temperatures $T = 1.4$, 2, 4, 6, 10, 15, 20, 30, 50, and 70 K. (c) Coulomb gap as a function of charge carrier concentration. The background shows a schematic illustration of the Coulomb gap in the localized density of states (black shaded area). The red and blue areas, respectively, represent the electron and hole density of states, which overlap around the CNP.[30]

$$T_0 = \frac{ß e^2}{4\pi \varepsilon \varepsilon_0 k_B \xi}, \quad (2)$$

where ξ is the localization length, k_B the Boltzmann constant, ε_0 the vacuum permittivity, ε the dielectric constant of graphene, e the electron charge, and $\beta = 2.8$ a constant.[12] Values of the product $\varepsilon\xi$ calculated using this equation and the extracted T_0 values are included in Table I. Assuming a dielectric constant of $\varepsilon = 2.4$ for graphene on SiO_2,[13] a localization length of about 300 nm is obtained for sample no. 4 [cf. Fig. 1(a)]. The variation between the four 50-nm (hole diameter)/100-nm (hole spacing) cubical GAL samples, especially regarding the T_0 value, can be ascribed to variations in the nanohole dimensions due to the nonideal graphene etching step and different degrees of unintentional chemical functionalization of the hole edges. Also, the surface doping or related position of the CNP is important for the T_0 value, as will be shown below.

In addition, the hopping distance R_{hop} and hopping energy E_{hop} of the charge carriers, as well as the Coulomb gap E_{CG}, were calculated from T_0 using the following equations:[12,14,15]

$$R_{hop} = \frac{\xi}{4}\left(\frac{T_0}{T}\right)^{1/2}, \quad (3)$$

$$E_{hop} = \frac{1}{2}(T_0 T)^{1/2}, \quad (4)$$

$$E_{CG} = \frac{T_0}{ß\sqrt{4\pi}}. \quad (5)$$

The obtained values, collected in Table I, show three notable trends upon variation of the GAL geometry. Firstly, increasing the nanohole density through decreasing the nanohole spacing

(sample no. 1) results in a strong increase in T_0 and therefore a decrease in the product $\varepsilon\xi$. This change suggests a corresponding decrease of either the dielectric constant or the localization length or both. In Table I, ε is assumed to be constant. The hopping distance (at $T = 10$ K) is found to be about twice the separation between the nanoholes in the respective samples. With decreasing nanohole spacing, the hopping distance also decreases, as can be expected since the localized states at the nanohole edges move closer together. At the same time, the Coulomb gap (CG) increases as a result of the stronger localization and increased Coulomb interactions. The CG emerges as a linear gap[16] in the localized density of states between the two mobility edges at the border of the transport gap [see Fig. 1(c)]. The minimum of the CG is by definition always located at the Fermi energy. To probe the CG minimum as a function of charge carrier concentration, we performed measurements with applied back-gate voltage [see Fig. 2(a)]. It can be discerned that, with increasing electron or hole concentration, the CG is strongly reduced, indicating interactions become less important as more carriers are available for screening of the localized states. At moderate concentrations of $|n| \approx 2 \times 10^{11}$ cm^{-2}, the conductivity exponent changes from 1/2 to 1/3, such that the CG is no longer important below a value of $E_{CG} \approx 2$ K, and the

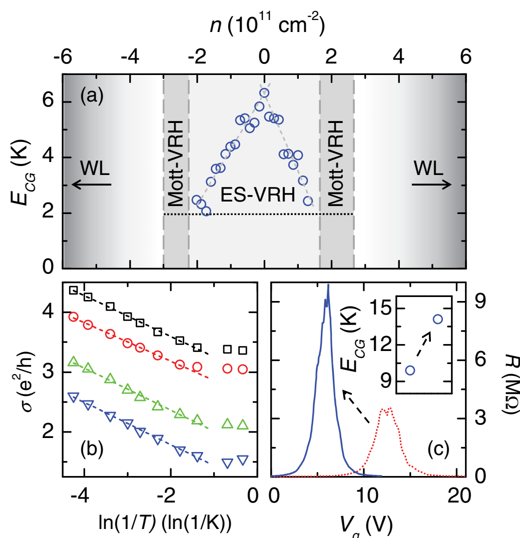

FIG. 2. (Color online) Concentration dependence of the Coulomb gap. (a) Close to the CNP the conduction is dominated by ES-VRH (sample no. 4). The extracted Coulomb gap decreases with increasing charge carrier concentration, in both the hole and electron regime. In the regimes -2.3×10^{11} cm^{-2} $< n < -3 \times 10^{11}$ cm^{-2} and 1.6×10^{11} cm^{-2} $< n < 2.7 \times 10^{11}$ cm^{-2}, the exponential fits (1) give an exponent close to $\nu = 1/3$, indicating transport is governed by Mott-VRH. For $|n| > 4 \times 10^{11}$ cm^{-2}, transport follows a weak localization (WL) behavior. (b) Temperature-dependent WL fits of sample no. 4 at $n = -4.0 \times 10^{11}$ cm^{-2} (blue triangles), -5.0×10^{11} cm^{-2} (green triangles), -6.1×10^{11} cm^{-2} (red circles), and -7.2×10^{11} cm^{-2} (black squares). Similar curves are obtained for the electrons. (c) Annealing sample no. 2 leads to a strong increase of the maximum resistance at the CNP and a shift closer to $V_g = 0$. The inset shows the increase of the Coulomb gap due to annealing. Measurements were performed at $T = 5.1$ K.

charge transport is governed by Mott-VRH without Coulomb interactions.[12] In the high-doping regime $|n| > 4 \times 10^{11}$ cm^{-2}, the temperature dependence of the conductance is no longer characteristic of VRH transport, but rather changes from exponential [Eq. (1), Fig. 1(a)] to logarithmic [Fig 2(b)], which is typical for weak localization:[17]

$$\sigma_{\mathrm{WL}} = -\frac{p}{\pi} \ln\left(\frac{T_0^{\mathrm{WL}}}{T}\right). \tag{6}$$

In this equation, p is the exponent for the temperature dependence of the phase breaking rate, $\tau_\phi^{-1} = \alpha T^p$ with α being a constant, and $T_0^{\mathrm{WL}} = (D/al^2)^{1/p}$ with D the diffusion constant and l the charge carrier mean free path. Hence, upon increasing the carrier concentration, the GALs undergo a transition from a strongly localized to a weakly localized regime. At low temperatures $T < 4$ K, we observe a small deviation from the weak localization behavior [Fig. 2(b)], which we attribute to the onset of VRH. Fitting the temperature dependence at high concentrations [$|n| > 4 \times 10^{11}$ cm^{-2}, see Fig. 1(b)] with Eq. (6) yields $p = 1.07 \pm 0.07$, corresponding to a temperature dependence of the phase coherence length of $L_\phi \propto \tau_\phi^{1/2} \propto T^{-0.5}$. This dependency is in good agreement with the values found for graphene[18] and for heavily doped GALs.[10]

The second trend observable in Table I is a drop of the exponent ν from ~0.5 to ~0.26 (sample no. 7) upon decreasing the nanohole density by increasing the dot spacing. This change suggests a transition toward Mott variable range hopping (Mott-VRH) in two dimensions, which is characterized by an exponent of 1/3 for a two-dimensional system.[12] It is noteworthy that a similar transition has been documented for graphene covalently functionalized with fluorine,[19] albeit the functionalization pattern is quite likely more random compared to the present samples. In fluorinated graphene, charge transport was found to occur via ES-VRH at higher functionalization degrees (equivalent to a high density of localized states), whereas at lower fluorine content, the transport was dominated by Mott-VRH. Such a transition is in accordance with theory predicting that for lower densities of localized states, the average hopping distance increases, and correspondingly the Coulomb gap becomes less relevant, and a constant density of states g_0 prevails.[15,19]

The third remarkable trend in Table I relates to the effect of sample annealing, which was performed at 125 °C for 4 h with the aim of removing surface contaminants (mostly water). As apparent from Fig. 2(c), the annealed sample no. 2 exhibits a strong increase of the resistance maximum, and the CNP is shifted closer to zero gate voltage. Concomitantly, there is a strong increase of T_0, which in turn leads to an enhanced CG. These observations suggest that also the unintentional doping atoms at the graphene surface have a profound influence on the strength of the Coulomb interactions and cause weaker localization similar to the effect of increasing the carrier concentration via the back gate. Highly doped GALs[10] are therefore expected to show weak localization behavior instead of the strong localized VRH observed in our samples.

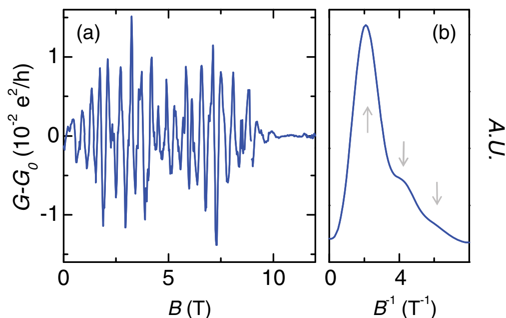

FIG. 3. (Color online) Aharonov–Bohm oscillations in GALs. (a) Aharonov–Bohm oscillations in sample no. 6 at $T = 1.4$ K and $V_g = V_{\mathrm{CNP}} + 0.3$ V, where G_0 is the smoothly varying background subtracted from the raw conductance data (G) to visualize the oscillations. (b) Corresponding FFT of the oscillations, displaying clear maxima at $eA/h = 2.1$ and $2eA/h \approx 4.2$ and a third, weak maximum at $2eA/h \approx 6.3$.

C. Transport in graphene antidot lattices at $B \neq 0$ T

In order to further evaluate the charge transport mechanism in the GALs, we measured their electrical resistance under applied magnetic field. First, we address the transport properties at high magnetic fields between 2 and 10 Tesla, where the conductance is of the order of e^2/h, and charge transport no longer occurs via VRH. In this regime, the resistance shows an oscillatory behavior as a function of magnetic field [see Fig. 3(a)], which can be ascribed to Aharonov–Bohm-(AB) type oscillations around the individual nanoholes.[20,21] In general, the AB oscillations were found to be most prominent around the CNP, while upon varying the back-gate voltage, the oscillation period changed only slightly in a sample-dependent manner. The AB oscillation period is given by $\Delta B = \varphi_0/A$,[22] with $\varphi_0 = h/e$ representing the flux quantum and A being the area enclosed by the charge carrier moving around the hole. For sample no. 6, an oscillation period of $\Delta B = 0.48$ T is obtained [see Figs. 3(a) and 3(b)], which agrees well with a closed path around the individual nanoholes with an AB diameter of 105 nm. Besides the first harmonic, the second and weak third harmonic can be discerned at $1/B \approx 4.2$ T^{-1} and $1/B \approx 6.3$ T^{-1} [Fig. 4(c)], respectively, which is ascribable to charge carriers which move a second (third) time phase coherently around the hole. This yields an estimate of the phase coherence length as three times half the circumference of the closed paths, corresponding to a value of $L_\varphi \approx 495$ nm. In the same manner, a phase coherence length of $L_\varphi \approx 375$ nm is derived for sample no. 4. Similar values have recently been gained from magnetoresistance oscillations in GALs prepared on SiC (~100 nm at 1 K).[21]

Next, we take a closer look at the magnetoresistance behavior at the CNP at sufficiently low B fields to be still within the VRH regime. In Fig. 4(a), the magnetoresistance is plotted for three different samples at the CNP for magnetic fields up to 4 Tesla. The bare graphene device (sample no. 8) shows a small positive magnetoresistance. A similar behavior is observed for the cubic GAL with 200-nm nanohole spacing (sample no. 7), although it displays an appreciably stronger resistance increase at higher magnetic fields. The cubic GAL with 100-nm spacing (sample no. 6) also shows a similar

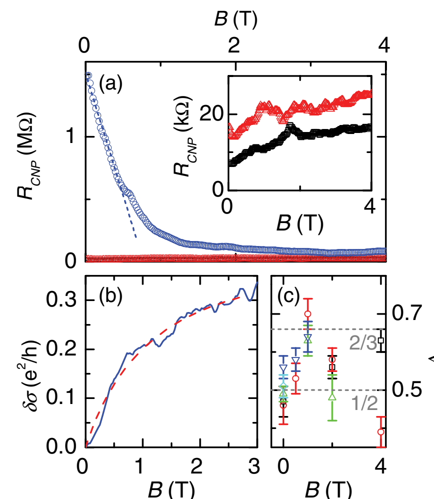

FIG. 4. (Color online) Magnetoresistance of several GAL devices. (a) Resistance at the CNP as a function of magnetic field for the bare graphene sample (sample no. 8, black squares), the 200-nm spacing antidot sample (sample no. 7, red triangles), and a 100-nm spacing antidot sample (sample no. 6, blue circles). All curves were measured at $T = 1.4$ K. The dotted line shows a linear fit to the low field dependency of sample no. 6. The inset shows a zoom of the main panel. (b) Magnetic field dependence of the conductivity correction in sample no. 5 in the weak localization regime ($n = -4.0 \times 10^{11}$ cm^{-2}), the red dashed line is a weak localization fit.[10] (c) Plot of the exponent ν, extracted from Eq. (1), for all the samples as a function of the B field, sample 1 (black squares), sample 3 (red circles), sample 4 (green up triangles), sample 5 (blue down triangles), and sample 6 (cyan diamonds). The dashed lines are guides to the eye.

positive magnetoresistance at moderate magnetic fields, but is combined with a pronounced quasilinear resistance decrease at magnetic fields below ~1 Tesla. A similar dependency in the VRH regime was found for the other samples with 100-nm spacing (no. 2, 3, 4, 5), as well as sample no. 1 with 80-nm spacing. The pronounced, quasilinear negative magnetoresistance observed for all these samples at lower magnetic fields is indicative of a strong change in the hopping probability.[23,24] The hopping probability is determined by interference between many paths connecting localized states at sites A and B separated by the hopping distance R_{hop}. Numerical averaging of the logarithm of the conductivity over many random impurities leads to a net linear decrease of the resistance with magnetic field above a threshold field $B_c = h/(2\pi e R_{\mathrm{hop}}^{3/2}\xi^{1/2})$, while for lower field strengths the MR depends on B^2.[25] In the specific case of sample no. 6, this threshold field is calculated to be $B_c = 6$ mT, which is below the minimum applicable value in our experiments, thus explaining why a purely linear B-field dependence is visible in Fig. 4(a). The negative linear MR is characterized by the flux penetrating an area A_{nMR} of the order of ${R_{\mathrm{hop}}}^{3/2}\xi^{1/2}$.[24] For samples no. 6 and 4, this implies that, in order for this interference effect to be observable, a charge carrier needs to be phase coherent around half the circumference of this area A_{nMR}, corresponding to ~580 and ~390 nm, respectively. This length, although determined in a different magnetic field range, is in reasonable agreement with the extracted phase coherence lengths $L_\varphi \approx 500$ nm (sample no. 6) and $L_\varphi \approx 375$ nm (sample no. 4), as

derived from Aharonov–Bohm (AB) oscillations observed at high magnetic fields.[22] At high carrier concentrations $|n| > 4 \times 10^{11}$ cm^{-1}, i.e. within the weak localization regime, the magnetoresistance shows a similar, albeit considerably weaker negative MR. This nMR or positive magnetoconductance can be reasonably described by a weak localization correction to the conductivity [see Fig. 4(b)], in analogy to highly doped GALs.[10] Fitting the weak localization data of sample no. 5 [dashed red line in Fig. 4(b)] yields a phase coherence length in the weak localization regime of $L_\phi = 20$ nm, an intervalley scattering length of $L_i = 11$ nm and a scattering length of $L_* = 3$ nm. These values are in reasonable agreement with weak localization measurements on highly doped GALs with similar dimensions.[10] One plausible explanation for the discrepancy between the phase-coherence length obtained from the VRH regime and the WL regime is the considerably higher density of induced charge carriers in the latter. These charges are expected to screen localized states and thus render long phase-coherent hops between them unlikely. This picture is in agreement with the fact that, in our experiments, we did not observe any B-dependent (AB-type) oscillations in the WL regime.

Furthermore, we explored the temperature dependence of the conductance at the CNP under constant magnetic field. Analogous to the analysis in Figs. 1(a) and 1(b), the temperature-dependent conductivity curves taken at magnetic fields $B = 0$, 0.5, 1, 2, and 4 T were fitted using Eq. (1) with T_0 and the exponent ν as a fitting parameter. In Fig. 4(c), the exponent ν obtained in this manner is plotted as a function of applied magnetic field. With rising magnetic field, the exponent is seen to increase from a value of $\sim 1/2$ to $\sim 2/3$, followed by a decrease back toward 1/2. The observed initial increase to an exponent of 2/3 is consistent with predictions by percolation theory applied to ES-VRH within a 2D system,[26] according to which the conductivity under applied magnetic field is given by

$$\sigma = \sigma_0 \exp\left(\frac{T_{0,B}}{T}\right)^{\frac{2}{3}}, \tag{7}$$

where $T_{0,B} = te^2/4\pi\varepsilon_0\varepsilon k_B l_B$. In the latter equation, t is a constant, and $l_B = \sqrt{(\hbar/eB)}$ is the magnetic length. It is noteworthy that in previous charge transport studies of semiconductor 2DEGs, this transition could not be observed, as it was most likely obscured by the predominance of Mott-VRH within this B-field range.[12,27,28] The extracted $T_{0,B}$ values are quite low, respectively, 17 ± 1 K (at $B = 1$ T) for samples 3–5 and 81 ± 10 K (at $B = 4$ T) for sample 1. These results could be validated by fitting Eq. (6) to the magnetic field-dependent transport data in a different way, i.e. using fixed T and variable B [see e.g. Fig. 4(a)]. In the relevant magnetic field range between 0.5 and 1.5 Tesla, the logarithm of the conductance depends linearly on $B^{1/3}$, which according to Eq. (6) yields $T_{0,B} = 16 \pm 2$ K (at $T = 1.4$ K and $B = 1$ T) for the same samples, in close agreement with the above values obtained from the temperature-dependent fits of Eq. (6). Assuming a comparable dielectric constant for the GAL samples and pristine graphene,[8] the low values of $T_{0,B}$ indicate that the constant t is notably reduced due to, for example, the influence of quantum interference effects.[26] This scenario gains support from the observed strong negative magnetoresistance as well as theoretical studies indicating a significant influence of an applied magnetic field on the hopping probability.[29]

The observation that, at higher magnetic fields (>2 Tesla), the exponent of $\nu = 1/2$ is resumed is characteristic of VRH in 2D systems and has been commonly ascribed to a transition from ES-VRH to Mott-VRH.[15,26–28] The increased B field is required to sufficiently reduce the Coulomb interactions and render the Coulomb gap less influential. Under such a condition, ES-VRH can only be recovered by lowering the temperature.[12,14,15] Another effect of the magnetic field is shrinkage of the wave function, which leads to weak positive magnetoresistance, as observed in our experiments [cf. Fig. 4(a)].

III. CONCLUSION

In summary, by studying a set of graphene antidot lattices with different geometry, we showed that a transport gap is opened whose characteristics depend on the nanohole arrangement, the strength of an externally applied magnetic field, as well as the charge carrier density in the patterned sheets. Specifically, up to a magnetic field of 1 Tesla, charge transport is governed by Efros–Sklovski (ES) VRH between localized states inside the gap, reflecting the importance of Coulomb interactions. Upon increasing the B field, the hopping conduction displays a transition from ES- to Mott-type between 1 and 2 Tesla. This transition can alternatively be induced by increasing the charge carrier concentration or the nanohole spacing in the samples.

ACKNOWLEDGMENTS

The authors are grateful to C. F. J. Flipse for valuable discussions.

*Corresponding author: a.j.m.giesbers@tue.nl; current address: Molecular Materials and Nanosystems, Eindhoven University of Technology, NL-5600 MB Eindhoven, The Netherlands.

[1] A. K. Geim and K. S. Novoselov, Nat. Mater. **6**, 183 (2007).

[2] A. K. Geim, Science **324**, 1530 (2009).

[3] X. Wang, Y. Ouyang, X. Li, H. Wang, J. Guo, and H. Dai, Phys. Rev. Lett. **100**, 206803 (2008).

[4] J. Bai, R. Cheng, F. Xiu, L. Liao, M. Wang, A. Shailos, K. L. Wang, Y. Huang, and X. Duan, Nature Nanotechnol. **5**, 655 (2010).

[5] J. A. Furst, T. G. Pedersen, M. Brandbyge, and A. P. Jauho, Phys. Rev. B **80**, 115117 (2009).

[6] M. Vanevic, V. M. Stojanovic, and M. Kindermann, Phys. Rev. B **80**, 045410 (2009).

[7] M. Begliarbekov, O. Sul, J. J. Santanello, N. Ai, X. Zhang, E. H. Yang, and S. Strauf, Nano Lett. **11**, 1254 (2011).

[8]J. A. Furst, J. G. Pedersen, C. Flindt, N. A. Mortensen, M. Brandbyge, T. G. Pedersen, and A. P. Jauho, New J. Phys. **11**, 095020 (2009).
[9]H. Jippo, M. Ohfuchi, and C. Kaneta, Phys. Rev. B **84**, 075467 (2011).
[10]J. Eroms and D. Weiss, New J. Phys. **11**, 095021 (2009).
[11]K. S. Novoselov, A. K. Geim, S. V. Morozov, D. Jiang, Y. Zhang, S. V. Dubonos, I. V. Grigorieva, and A. A. Firsov, Science **306**, 666 (2004).
[12]B. I. Shklovskii and A. L. Efros, *Springer Series in Solid-State Sciences*, edited by M. Cardona, P. Fulde, and H.-J. Queisser (Springer-Verlag, Berlin, 1984), Vol. 45.
[13]K. W. K. Shung, Phys. Rev. B **34**, 979 (1986).
[14]S. J. Lee, J. B. Ketterson, and N. Trivedi, Phys. Rev. B **46**, 12695 (1992).
[15]R. Rosenbaum, Phys. Rev. B **44**, 3599 (1991).
[16]C. J. J. Adkins, J. Phys.: Condens. Matter **1**, 1253 (1989).
[17]B. Kramer and A. MacKinnon, Rep. Prog. Phys. **86**, 1469 (1993).
[18]S. V. Morozov, K. S. Novoselov, M. I. Katsnelson, F. Schedin, L. A. Ponomarenko, D. Jiang, and A. K. Geim, Phys. Rev. Lett. **97**, 016801 (2006).
[19]F. Withers, S. Russo, M. Dubois, and M. F. Craciun, Nanoscale Res. Lett. **6**, 526 (2011).
[20]D. Weiss, K. Richter, A. Menschig, R. Bergmann, H. Schweizer, K. von Klitzing, and G. Weimann, Phys. Rev. Lett. **70**, 4118 (1993).
[21]T. Shen, Y. Q. Wu, M. A. Capano, L. P. Rokhinson, L. W. Engel, and P. D. Ye, Appl. Phys. Lett. **93**, 122102 (2008).
[22]Y. Aharonov and D. Bohm, Phys. Rev. **115**, 485 (1959).
[23]W. Schirmacher, Phys. Rev. B **41**, 2461 (1990).
[24]U. Sivan, O. Entin-Wohlman, and Y. Imry, Phys. Rev. Lett. **60**, 1566 (1988).
[25]V. I. Nguyen, B. Z. Spivak, and B. I. Shlovskii, JEPT Lett. **41**, 42 (1985); Sov. Phys. JEPT **62**, 1021 (1985).
[26]N. Van Lien, Phys. Lett. A **207**, 379 (1995).
[27]B. Capoen, G. Biskupski, and A. Briggs, Solid State. Commun. **113**, 135 (2000).
[28]M. Iqbal, J. Galibert, J. Léotin, S. Waffenschmidth, and H. von Löhneysen, Philos. Mag. Part B **79**, 1591 (1999).
[29]E. Medina and M. Kardar, Phys. Rev. B **46**, 9984 (1992).
[30]S. Wiedmann, H. J. van Elferen, E. V. Kurganova, M. I. Katsnelson, A. J. M. Giesbers, A. Veligura, B. J. van Wees, R. V. Gorbachev, K. S. Novoselov, J. C. Maan, and U. Zeitler, Phys. Rev. B **84**, 115314 (2011).